Eur. Phys. J. B **9**, 513–524 (1999)

THE EUROPEAN PHYSICAL JOURNAL B

EDP Sciences

Coherent resonant transport through a mesoscopic system with quantum ac microwave field

H.-K. Zhao[1,2,a] and J. Wang[1]

[1] Department of Physics, The University of Hong Kong, Pokfulam Road, Hong Kong, China
[2] Department of Physics, Beijing Institute of Technology, Beijing 100081, China

Received 28 may 1998

Abstract. The time-dependent transport through an ultrasmall quantum dot coupling to two electron reservoirs is investigated. The quantum dot is perturbed by a quantum microwave field (QMF) through gate. The tunneling current formulae are obtained by taking expectation values over coherent state (CS), and SU(1,1) CS. We derive the transport formulae at low temperature by employing the nonequilibrium Green function technique. The currents exhibit coherent behaviors which are strongly associated with the applied QMF. The time-dependent currents appear compound effects of resonant tunneling and time-oscillating evolution. The time-averaged current and differential conductance are calculated, which manifest photon-assisted behaviors. Numerical calculations reveal the similar properties as those in classical microwave field (CMF) perturbed system for the situations concerning CS and squeezed vacuum SU(1,1) CS. But for other squeezed SU(1,1) CS, the tunneling behavior is quite different from the system perturbed by a single CMF through gate. Due to the quantum signal perturbation, the measurable quantities fluctuate fiercely.

PACS. 73.40.-c Electronic transport in interface structures – 73.20.Dx Electron states in low-dimensional structures (superlattices, quantum well structures and multilayers) – 72.10.Bg General formulation of transport theory

1 Introduction

The investigation on transport through mesoscopic systems develops very rapidly in the past few years both in theoretical and experimental aspects [1-8]. The reason why this prosperous field attracts so much attention is that it has potential applications in electronic industry. The quantum devices are composed of small sample whose dimensions are comparable with or much smaller than the coherence lengths of electron. These devices possess different microstructures which can be described by two-dimensional electron gas confined in small samples. In another dimension electrons can tunnel through the device from source to drain, and they are controlled by appropriate gate voltages. Electrons transport through such small devices exhibit interesting phenomena due to phase coherence and confinement. The Coulomb interaction is important, and the single-particle spectrum is discrete in these systems. The Coulomb interaction and the geometry of a device may cause the phenomenon known as the Coulomb blockade [9,10]. Quantum dots are the models to describe these small quantum devices which are characterized by small capacitances to the substrate and to the leads.

In the past years, transports through quantum devices with dc voltages applying to them are investigated intensively, and many properties have been understood now. Recently, the time-dependent transport through small quantum devices attracted much interest, and it becomes a very active research frontier. In fact, high-frequency signals may be applied to the quantum devices, and information of applied fields will be transferred to the tunneling currents. Some novel phenomena, such as photon-assisted tunneling [11-18], photon-electron pump effect [19,20], have been observed. During the transport, electrons absorb or emit photons to split the single electron spectrum. The transport shows resonant peaks induced by the sideband around the main resonant peak. If an electron absorbs enough energy from photons, it can overcome thresholds and then transport to the other lead. Comparing with the dc transport, the time-dependent transport is still in its immature stage. The theoretical investigation on time-dependent tunneling can be traced back to the work performed by Tien and Gordon [21]. They studied the single electron tunneling through superconductor films with classical microwave fields (CMFs). They explained the two phenomena: the excess of tunneling current, and the current appearing voltage steps. As a CMF is applied, electric field $\mathbf{E}(\mathbf{r},t)$ and vector potential $\mathbf{A}(\mathbf{r},t)$ may affect the motions of electrons in the sample. The fields are location-dependent in general. However, if the system is very small, and the wavelength

[a] e-mail: zhaohonk@public.east.cn.net

of the field is large enough, we can approximate the variation of the field to consider it as space-independent one. In the dipole approximation and by neglecting the effect of all other fields, the electric field sets up a potential difference $V_0\cos(\omega t)$ between two films. With CMFs applying to the system, an electron tunneling through a quantum device may exchange energy with the external fields, so that its phase will be modified. The external time-dependent perturbation affects the phase coherence differently in different parts of the system [22]. In the classical region ($\hbar\omega \ll k_{\rm B}T$), the quantum effect is not obvious, while in the quantum region ($\hbar\omega \gg k_{\rm B}T$) the tunneling current shows obvious effect of photon absorption and emission. Theoretically, the quantum devices are so small that their sizes L lie in the phase coherence regime $L \leq L_\phi$, where L_ϕ is the coherence length. Quantum mechanical rules govern the movement of electrons. As microwave fields apply to the mesoscopic systems, new quantum effect may be induced if we deal with the problems in fully quantum point of view by considering the microwave fields as non-classical versions. To exploit the full quantum mechanical nature of mesoscopic Josephson junctions, Vourdas has proposed a theory to describe the interaction between the device and the quantum fields, and some new properties were found by Kuang *et al.* [23].

In this paper, we study the system composed of a quantum dot coupling to two electron reservoirs with a quantum microwave field (QMF) applying to the central dot through its gate. We study transport behaviors induced by the field as photon energy is much larger than thermal noise energy. In this system the current formula corresponding to the usual one becomes an operator, and the expectation value (EV) of current operator in a definite state of QMF is the observable quantity. For special cases, we consider coherent state (CS) and SU(1,1) CS to find EV of current. For simplicity, we deal with an ultrasmall quantum dot with single electron level. The dot is weakly coupled to source and drain reservoirs by tunneling junctions. This paper is organized as follows. Section 2 contains model description and transport formulae derivation. Sections 3 and 4 are devoted to the special cases for CS and SU(1,1) CS, respectively. We arrange some concluding remarks in Section 5.

2 Model and current formula

We investigate the system with quantum monochromatic field applying to the dot through its gate. Similar to the classical situation, QMF is location-dependent in general. For our system, the ultrasmall quantum dot is smaller than the order 10^{-6} m, while the wavelength of the QMF is larger than 10^{-4} m. So that $\mathbf{r}\cdot\mathbf{k} \ll 1$, and the QMF can be approximated as the space-invariant one, *i.e.*,

$$\mathbf{E}(t) = iE_0(c\mathrm{e}^{-i\omega t} - c^\dagger \mathrm{e}^{i\omega t}). \tag{1}$$

The Hamiltonian of the electromagnetic field in the monochromatic case is the harmonic oscillator Hamiltonian: $H_{\rm c} = \hbar\omega(c^\dagger c + \frac{1}{2})$, where $c^\dagger$ and c are the creation and annihilation operators of photon; ω is the angular frequency of the field. Because the velocity of an electron v in the quantum dot is much smaller than the speed of light C, *i.e.*, $v \ll C$, the magnetic force is much smaller than the electric force. This can be seen by comparing with the two forces

$$\frac{|\frac{e}{C}\mathbf{v}\times\mathbf{B}|}{|e\mathbf{E}|} \sim \frac{v}{C} \ll 1.$$

Thus, we neglect the effect of magnetic field, and merely consider the effect of electric field. This is associated with the dipole approximation. There is an upper limit of frequency in order to employ the nonequilibrium Green function technique. This upper limit can be up to tens of THz. As the frequencies of the external fields is smaller than this limit, we can use the adiabatic approximation to deal with the problems. For this circumstance, the external quantum field does not change the electronic distribution directly [22,24]. The effect of the quantum electric field is adding a dipole potential to the Hamiltonian of the system. To obtain self-consistent transport behaviors from this ac perturbed system one should consider induced potential by solving Helmhotz equation [25]. However, since we are mainly interested in the quantum effect caused by the QMF, and the induced potential is small comparing with the applied potential, we neglect the internal potential for simplicity [26]. Therefore, the Hamiltonian of the system is given by

$$\begin{aligned} H = &\sum_{\alpha\in\{\rm L,R\}}\sum_{k\sigma} E^\alpha_{k\sigma} a^\dagger_{\alpha,k\sigma} a_{\alpha,k\sigma} + \sum_\sigma [\hat{\varepsilon}_\sigma(t) n_{d\sigma} \\ &+ \frac{1}{2} U n_{d\sigma} n_{d-\sigma}] + \sum_{\alpha\in\{\rm L,R\}}\sum_{k\sigma} (T_{\alpha k} a^\dagger_{\alpha,k\sigma} d_\sigma + H.C.), \end{aligned} \tag{2}$$

where

$$\hat{\varepsilon}_\sigma(t) = E_{d\sigma} + i\Delta_d(c\mathrm{e}^{-i\omega t} - c^\dagger \mathrm{e}^{i\omega t}).$$

In equation (2), $a^\dagger_{\alpha,k\sigma}(a_{\alpha,k\sigma})$ and $d^\dagger_\sigma(d_\sigma)$ are the creation (annihilation) operators of electron in the αth lead and in the quantum dot respectively with momentum k and spin σ. $E^\alpha_{k\sigma}$, and $E_{d\sigma}$ are single electron energy levels corresponding to the αth lead and the quantum dot. $n_{d\sigma}$ is the number operator of electron in the dot. The intra-dot Coulomb interaction is described by the strength U. The effect of time-dependent QMF is contained in $\hat{\varepsilon}_\sigma(t)$. The coupling strength between the field and quantum dot is given by Δ_d. We assume that the coupling strength Δ_d is so small that there is no nonlinear turbulence behavior or non-physical divergence arising from the perturbation.

We employ the Keldysh nonequilibrium Green function technique [22,27,28] to derive the current formula. In the presence of the external oscillating perturbations, the current is time-dependent, and it is different from point to point due to the accumulation of electrons. The current at a point is the differences between the flow of electrons

from opposite directions. The charge operator in the αth lead is $\rho_\alpha = \sum_{k\sigma} a^\dagger_{\alpha,k\sigma} a_{\alpha,k\sigma}$. According to the continuity equation and Heisenberg equation, we have the operator of current flowing into the quantum dot from the αth lead [22]

$$\hat{I}_\alpha(t) = -\frac{ie}{\hbar}\sum_{k\sigma}\langle[H, a^\dagger_{\alpha,k\sigma}(t)a_{\alpha,k\sigma}(t)]\rangle, \alpha \in \{\mathrm{L},\mathrm{R}\}. \quad (3)$$

The symbol $\langle ...\rangle$ in above formula denotes the quantum expectation over the electron state, and the ensemble average over the system. In order to find the observable current, one still needs to find EV over a QMF state. The Hamiltonian H in equation (3) is defined by equation (2). Substitute the Hamiltonian into the current formula, one can verify that the following formula shown in reference [22] is still valid in our QMF perturbed system

$$\hat{I}_\alpha(t) = \frac{2e}{\hbar}\mathrm{Re}\{\sum_{k\sigma} T_{\alpha k}\langle\langle d_\sigma(t)a^\dagger_{\alpha,k\sigma}(t)\rangle\rangle^<\}, \alpha \in \{\mathrm{L},\mathrm{R}\}, \quad (4)$$

where $\langle\langle d_\sigma(t_1)a^\dagger_{\alpha,k\sigma}(t_2)\rangle\rangle^< = i\langle a^\dagger_{\alpha,k\sigma}(t_2)d_\sigma(t_1)\rangle$. However, the current formula defines a quantum operator of current in the QMF Fock space. Because the leads are described by free electron grand ensemble, we can express the Keldysh Green function by the Dyson equation. In the Dyson equation, $g^<_{\alpha,k\sigma}(t_1,t_2)$ and $g^a_{\alpha,k\sigma}(t_1,t_2)$ are the Keldysh and advanced Green functions of the αth lead. The Fourier transformed versions of these Green functions are expressed as $g^<_{\alpha,k\sigma}(\epsilon) = 2\pi i f_\alpha(\epsilon)\delta(\epsilon - E^\alpha_{k\sigma})$, and $g^{r(a)}_{\alpha,k\sigma}(\epsilon) = (\epsilon - E^\alpha_{k\sigma} \pm i\eta)^{-1}$. $\hat{G}^r_{d\sigma}(t_1,t_2)$ and $\hat{G}^<_{d\sigma}(t_1,t_2)$ are denoted as the retarded and Keldysh Green function operators of the quantum dot. In the presence of time-dependent perturbations, the time-translation invariance of the Green function is broken. In our system, this signifies $\hat{G}^X_{d\sigma}(t_1,t_2) \neq \hat{G}^X_{d\sigma}(t_1 - t_2)$. Substitute the Dyson equation into current formula (4), one obtains the time-dependent current operator expressed by the Green function operators of quantum dot and the Green functions of two leads [22]

$$\hat{I}_\alpha(t) = -\frac{2e}{h}\sum_\sigma\int_{-\infty}^{t}\mathrm{d}t'\int\mathrm{d}\epsilon\,\mathrm{Im}\{\mathrm{e}^{\frac{i}{\hbar}\epsilon(t-t')}\Gamma^\alpha(\epsilon) \times [\hat{G}^<_{d\sigma}(t,t') + f_\alpha(\epsilon)\hat{G}^r_{d\sigma}(t,t')]\}, \quad (5)$$

where $\Gamma^\alpha(\epsilon) = 2\pi\sum_k \mid T_{\alpha k}\mid^2 \delta(\epsilon - E^\alpha_{k\sigma})$ is the linewidth. The Green function operators of the quantum dot is defined by $\hat{G}^r_{d\sigma}(t,t') = -\frac{i}{\hbar}\theta(t-t')\langle\{d_\sigma(t), d^\dagger_\sigma(t')\}\rangle$, and $\hat{G}^<_{d\sigma}(t,t') = \frac{i}{\hbar}\langle d^\dagger_\sigma(t')d_\sigma(t)\rangle$.

To proceed the calculations, we define an operator $\hat{Q}(t)$ as

$$\hat{Q}(t) = \hat{X}_1\cos(\omega t) + \hat{X}_2\sin(\omega t), \quad (6)$$

where

$$\hat{X}_1 = \frac{1}{2}(c + c^\dagger), \hat{X}_2 = \frac{1}{2i}(c - c^\dagger).$$

The operators $\hat{X}_1$, $\hat{X}_2$ and $\hat{Q}(t)$ satisfy the commutation relations $[\hat{X}_1, \hat{X}_2] = i/2$, and $[\hat{Q}(t_1), \hat{Q}(t_2)] = -\frac{i}{2}\sin[\omega(t_1 - t_2)]$. Obviously, the operator $\hat{Q}(t)$ is an Hermitian operator which satisfies $\hat{Q}(t)^\dagger = \hat{Q}(t)$. Using the commutation relations between the operators $Q(\hat{t}_1)$ and $Q(\hat{t}_2)$, one can derive the relation

$$\hat{P}^\dagger(t_2)\hat{P}(t_1) = \hat{P}(t_1)\hat{P}^\dagger(t_2)\zeta^2(t_1,t_2), \quad (7)$$

where

$$\zeta(t,t') = \exp\{\frac{i}{4}\lambda^2\sin[\omega(t_1 - t_2)]\},$$
$$\hat{P}(t) = \exp[i\lambda\hat{Q}(t)], \lambda = \frac{2\Delta_d}{\hbar\omega}.$$

Similar to the scattering theory, we deal with the transport problem by separating the system into three regions. The central quantum dot acts as the scatterer of electrons ejected from electron reservoirs. The electrons interact with the local electrons in the quantum dot by the coupling strength $T_{\alpha k}$. All the Green functions in the quantum dot should be calculated by solving the coupled system in the presence of tunneling. $\hat{G}^<_{d\sigma}$ depends on the occupation in the leads, and $\hat{G}^{r(a)}_{d\sigma}$ depends on the central region occupation. Similar to the system perturbed by CMF [29], we make the gauge transform for the operator $d_\sigma(t)$ in the second order quantized state vector in Hilbert space for local electron as

$$d_\sigma(t) = \hat{P}(t)\tilde{d}_\sigma(t), \quad (8)$$

where $\tilde{d}_\sigma(t)$ is a new annihilation operator of electron in the quantum dot. By the transformation, the time-dependent energy $\hat{\epsilon}_\sigma(t)$ changes to the time-independent $E_{d\sigma}$, but the interaction strength $T_{\alpha k}$ changes to $T_{\alpha k}\hat{P}(t)$. Therefore, the Hamiltonian (2) is transformed to the following form by making the gauge transformation

$$\tilde{H} = \sum_{\alpha\in\{\mathrm{L},\mathrm{R}\}}\sum_{k\sigma} E^\alpha_{k\sigma}a^\dagger_{\alpha,k\sigma}a_{\alpha,k\sigma} + \sum_\sigma[E_{d\sigma}\tilde{n}_{d\sigma} + \frac{1}{2}U\tilde{n}_{d\sigma}\tilde{n}_{d-\sigma}] + \sum_{\alpha\in\{\mathrm{L},\mathrm{R}\}}\sum_{k\sigma}\{T_{\alpha k}\hat{P}(t)a^\dagger_{\alpha,k\sigma}\tilde{d}_\sigma + T^*_{\alpha k}\hat{P}^\dagger(t)\tilde{d}^\dagger_\sigma a_{\alpha,k\sigma}\}, \quad (9)$$

where $\tilde{n}_{d\sigma} = \tilde{d}^\dagger_\sigma\tilde{d}_\sigma$. The Green function operators $\hat{\tilde{G}}^<_{d\sigma}(t_1,t_2)$ and $\hat{\tilde{G}}^{r(a)}_{d\sigma}(t_1,t_2)$ are defined as follows

$$\hat{\tilde{G}}^<_{d\sigma}(t_1,t_2) = \frac{i}{\hbar}\langle\tilde{d}^\dagger_\sigma(t_2)\tilde{d}_\sigma(t_1)\rangle, \quad (10)$$

$$\hat{\tilde{G}}^{r(a)}_{d\sigma}(t_1,t_2) = \mp\frac{i}{\hbar}\theta(\pm t_1 \mp t_2)\langle\{\tilde{d}_\sigma(t_1), \tilde{d}^\dagger_\sigma(t_2)\}\rangle. \quad (11)$$

The current operator $\hat{I}_\alpha(t)$ now can be written in the following form by making gauge transformation and by using Dyson equation with the Hamiltonian given

by equation (9) that

$$\hat{I}_\alpha(t) = -\frac{2e}{h}\mathrm{Im}\sum_\sigma \int_{-\infty}^{t} \mathrm{d}t' \int \mathrm{d}\epsilon \Gamma_\alpha(\epsilon)\hat{P}(t)\hat{P}^\dagger(t')\mathrm{e}^{\frac{i}{\hbar}\epsilon(t-t')} \times [\hat{\tilde{G}}^{<}_{d\sigma}(t,t') + f_\alpha(\epsilon)\hat{\tilde{G}}^{r}_{d\sigma}(t,t')]. \quad (12)$$

The productor of two operators $\hat{P}(t_i)$ can be expressed by the usual displacement operator $\hat{D}(\alpha)$ as

$$\hat{P}(t_1)\hat{P}^\dagger(t_2) = \hat{D}(\alpha)\zeta(t_2,t_1) \quad (13)$$

where

$$\hat{D}(\alpha) = \exp(\alpha c^\dagger - \alpha^* c),$$

$$\alpha = \frac{i}{2}\lambda[\exp(i\omega t_1) - \exp(i\omega t_2)].$$

The EV of an operator $\hat{O}(t_1,t_2)$ over a certain QMF state is defined by

$$\langle \hat{O}(t_1,t_2)\rangle = \mathrm{Tr}\{\hat{\rho}\hat{O}(t_1,t_2)\}, \quad (14)$$

with the density matrix $\hat{\rho}$ describing the QMF. The Green functions $\tilde{G}^X_{d\sigma}(t,t')$ are therefore given by EV of the Green function operators $\hat{\tilde{G}}^{X}(t,t')$ over special state, *i.e.*, $\tilde{G}^X_{d\sigma}(t,t') = \langle\hat{\tilde{G}}^{X}_{d\sigma}(t,t')\rangle$,where $X \in \{r,a,<\}$.

The Keldysh Green function $\tilde{G}^<_{d\sigma}$ can be calculated by the formula given in reference [22], and by employing the relations for the Bessel function of the first kind $J_n(\tau)$, and the modified Bessel function of the first kind $I_n(\tau)$ as

$$\exp(-i\xi\sin\alpha) = \sum_{n=-\infty}^{\infty} J_n(\xi)\exp(-in\alpha),$$

$$\exp(\pm i\xi\cos\alpha) = \sum_{n=-\infty}^{\infty} (\pm i)^n J_n(\xi)\exp(in\alpha),$$

$$\exp(\xi\cos\alpha) = \sum_{n=-\infty}^{\infty} I_n(\xi)\exp(in\alpha).$$

We evaluate the Keldysh Green functions by using

$$\tilde{G}^<_{d\sigma}(t,t') = \iint \mathrm{d}t_1\mathrm{d}t_2 \tilde{G}^r_{d\sigma}(t,t_1)\tilde{\Sigma}^<(t_1,t_2)\tilde{G}^a_{d\sigma}(t_2,t'), \quad (15)$$

and the retarded Green function $\tilde{G}^r_{d\sigma}$ by the Dyson equation

$$\tilde{G}^r_{d\sigma}(t,t') = g^r_{d\sigma}(t,t') + \iint \mathrm{d}t_1\mathrm{d}t_2 g^r_{d\sigma}(t,t_1)\tilde{\Sigma}^r(t_1,t_2)\tilde{G}^r_{d\sigma}(t_2,t'). \quad (16)$$

In the above equations, $\tilde{\Sigma}^<$ and $\tilde{\Sigma}^r$ are the Keldysh and retarded self-energy of the central region with Hamiltonian defined by equation (9). For the noninteracting quantum dot where $U = 0$, they are expressed as

$$\tilde{\Sigma}^<(t_1,t_2) = \sum_{\alpha\in\{\mathrm{L,R}\}}\sum_k |T_{\alpha k}|^2 \langle\hat{P}^\dagger(t_1)\hat{P}(t_2)\rangle g^<_{\alpha,k\sigma}(t_1,t_2), \quad (17)$$

$$\tilde{\Sigma}^r(t_1,t_2) = \sum_{\alpha\in\{\mathrm{L,R}\}}\sum_k |T_{\alpha k}|^2 \langle\hat{P}^\dagger(t_1)\hat{P}(t_2)\rangle g^r_{\alpha,k\sigma}(t_1,t_2). \quad (18)$$

In the Dyson equation, $g^r_{d\sigma}$ is the retarded Green function of the quantum dot without connected to the two leads and in the absence of QMF. To elucidate the quantum effect of QMF in the mesoscopic system, we only consider the situation for the intradot Coulomb interaction is not important. So we set $U = 0$ for simplicity. We also focus on the wideband limit so that the Green functions are expressed exactly. In particular, transport is often dominated by states close to Fermi level, the wideband limit is a good approximation [22]. In this limit, level shift of the quantum dot is zero, and the linewidths are energy independent constants $\Gamma_\alpha(\epsilon) = \Gamma_\alpha$. Let $\Gamma_\mathrm{L} + \Gamma_\mathrm{R} = \Gamma$, the retarded self-energy is reduced to

$$\tilde{\Sigma}^r(t_1,t_2) = -\frac{i}{2}\Gamma\langle\hat{P}^\dagger(t_1)\hat{P}(t_2)\rangle\delta(t_1-t_2). \quad (19)$$

By noticing $\hat{P}^\dagger(t)\hat{P}(t) = 1$, we see that equation (19) is reduced to the simple form

$$\tilde{\Sigma}^r(t_1,t_2) = -\frac{i}{2}\Gamma\delta(t_1-t_2).$$

The Keldysh self-energy is given by

$$\tilde{\Sigma}^<(t_1,t_2) = i\int\frac{\mathrm{d}\epsilon}{2\pi}\Lambda(\epsilon)\exp[-\frac{i}{\hbar}\epsilon(t_1-t_2)]\langle\hat{P}^\dagger(t_1)\hat{P}(t_2)\rangle, \quad (20)$$

where

$$\Lambda(\epsilon) = \Gamma_\mathrm{L} f_\mathrm{L}(\epsilon) + \Gamma_\mathrm{R} f_\mathrm{R}(\epsilon).$$

Substitute the self-energy $\tilde{\Sigma}^r$ into equation (16) we find that the retarded (advanced) Green function $\tilde{G}^{r(a)}_{\mathrm{d}\sigma}$ appears as the one in the absence of external QMF

$$\tilde{G}^{r(a)}_{\mathrm{d}\sigma}(t,t') = \mp\frac{i}{\hbar}\theta(\pm t\mp t')\exp[-\frac{i}{\hbar}(E_{\mathrm{d}\sigma}\mp\frac{i}{2}\Gamma)(t-t')]. \quad (21)$$

In fact, at the wideband limit we have $\hat{\tilde{G}}^{r(a)}_{\mathrm{d}\sigma}(t,t') = \tilde{G}^{r(a)}_{\mathrm{d}\sigma}(t,t')$. Substitute the Green functions $\tilde{G}^r_{\mathrm{d}\sigma}, \tilde{G}^a_{\mathrm{d}\sigma}$ and the self-energy $\tilde{\Sigma}^<$ into equation (15), we can obtain the Keldysh Green function of the quantum dot described by the Hamiltonian (9) in a special QMF. We can find time-evolving current tunneling into the quantum dot from the αth lead by taking EV over certain QMF.

3 Coherent state expectation

We investigate the quantum state EV of current operator by using the CS light field in this section. This QMF state can be produced experimentally. Although this field is quantum electromagnetic field, it is not non-classical light field but the classical light field in the sense of quantum optics [30] due to the existence of positive definite nonsingular Glauber-Sudarshan P representation of its density operator. The CS is defined as the eigen state of the non-Hermitian operator c, *i.e.*, $c\,|\,Z\rangle = Z\,|\,Z\rangle$. In the number representation, it can be expressed as $|\,Z\rangle = \hat{D}(Z)\,|\,0\rangle$. Because the operator c is non-Hermitian, Z is a complex quantity. We take it as $Z = |Z|\mathrm{e}^{i\phi}$ for convenience. For the CS, we have the EV of the displacement operator $\hat{D}(\alpha)$ as

$$\langle z\,|\hat{D}(\alpha)|\,z\rangle = \exp(\alpha z^* - \alpha^* z - \frac{1}{2}\,|\alpha|^2). \tag{22}$$

For our system, α is given by equation (13) and the EV of the displacement operator is

$$\langle z\,|\hat{D}(\alpha)|\,z\rangle = \exp\{i\lambda\,|z|\,[\cos(\omega t-\phi)-\cos(\omega t'-\phi)] - \frac{\lambda^2}{4}[1-\cos(t-t')]\}. \tag{23}$$

The Keldysh Green function is evaluated in CS as

$$\tilde{G}^{<}_{d\sigma}(t,t') = i\mathrm{e}^{-\tau}\int\frac{\mathrm{d}\epsilon}{2\pi\hbar}\Lambda(\epsilon)\sum_{nm\ell p}(-1)^p i^{\ell+p}\mathrm{e}^{-i(\ell+p)\phi} \times J_n(\tau)J_\ell(\lambda\,|z|)J_p(\lambda\,|z|)I_m(\tau)F_{nm\ell p}(\epsilon,t,t'), \tag{24}$$

where

$$F_{nm\ell p}(\epsilon,t,t') = \exp\{-\frac{i}{\hbar}[\epsilon+(n+m)\omega(t-t') - \ell\omega t' - p\omega t]\}\tilde{G}^r_{d\sigma}[\epsilon+(n-p+m)\hbar\omega] \times \tilde{G}^a_{d\sigma}[\epsilon+(n+\ell+m)\hbar\omega],$$

and $\tau = \lambda^2/4$, $\tilde{G}^{r(a)}_{\mathrm{d}\sigma}(\epsilon) = (\epsilon - E_{\mathrm{d}\sigma} \pm i\Gamma/2)^{-1}$. The current $I_\alpha(t)$ is given by taking EV of the current operator $\hat{I}_\alpha(t)$ over CS, *i.e.*, $I_\alpha(t) = \langle\hat{I}_\alpha(t)\rangle$. In order to find the current, we have to calculate the EV of the tunneling current operator. As $\lambda \ll 1$, we make the approximation in our calculations to find the current in the αth lead

$$\langle\hat{P}(t)\hat{P}^\dagger(t')\hat{P}^\dagger(t_1)\hat{P}(t_1')\rangle \approx \langle\hat{P}(t)\hat{P}^\dagger(t')\rangle\langle\hat{P}^\dagger(t_1)\hat{P}(t_1')\rangle. \tag{25}$$

However, this approximation does not affect our evaluations for finding the nonequilibrium Green functions. It does not affect the net tunneling current transporting through the quantum dot if we consider the symmetric situation where $\Gamma_{\mathrm{L}} = \Gamma_{\mathrm{R}}$. It is not difficult to remove the approximation, and find exact result on the current formula. As $\lambda \ll 1$, and by making the approximation in equation (25), we immediately arrive at current formula in the αth lead

$$I_\alpha(t) = -\frac{2e}{h}\Gamma_\alpha\mathrm{Im}\{\eta(t)\sum_\sigma\int\mathrm{d}\epsilon\sum_{nm\ell}(-1)^\ell \times \mathrm{e}^{i\ell(\omega t-\phi+\pi/2)}J_\ell(\lambda\,|z|)J_n(\tau)I_m(\tau) \times [R_{n\ell m}(\epsilon,t)+f_\alpha(\epsilon)\tilde{G}^r_{d\sigma}(\epsilon-(n+\ell-m)\hbar\omega)]\}, \tag{26}$$

where

$$\eta(t) = \exp[-\tau + i\lambda\,|z|\cos(\omega t-\phi)],$$

$$R_{n\ell m}(\epsilon,t) = \frac{i}{2}\mathrm{e}^{-\tau}\sum_{n_1m_1\ell_1\ell_2}(-1)^{\ell_2}\Lambda[\epsilon-(n_1+\ell_1+m_1+n+\ell-m)\hbar\omega] \times \mathrm{e}^{i(\ell_1+\ell_2)(\omega t-\phi+\pi/2)}J_{n_1}(\tau)J_{\ell_1}(\lambda\,|\,z\,|)J_{\ell_2}(\lambda\,|\,z\,|)I_{m_1}(\tau) \times \tilde{G}^r_{d\sigma}[\epsilon-(\ell_1+\ell_2+n-m+\ell)\hbar\omega]\tilde{G}^a_{d\sigma}[\epsilon-(n-m+\ell)\hbar\omega].$$

The net tunneling current transporting through the quantum dot is the sum of the currents transporting from the two leads into the quantum dot, and the currents going out of the quantum dot transporting into the two leads. For the symmetric situation, the two parts of the currents going out of the quantum dot are cancelled. Therefore, the net current is given by $I(t) = \frac{1}{2}[I_{\mathrm{L}}(t) - I_{\mathrm{R}}(t)]$. We take the chemical potential of the left lead μ_{L} as the energy measurement reference, so that the measured energy of the quantum dot is $\tilde{E}_{\mathrm{d}} = E_{\mathrm{d}} - \mu_{\mathrm{L}}$. The potential drop between the two leads is defined by $\mu_{\mathrm{L}} - \mu_{\mathrm{R}} = eV$, where V is the measured voltage between the source and drain. At zero temperature the spin degenerate net tunneling current is reduced to the analytical form

$$I(t) = \frac{e}{h}\mathrm{e}^{-\tau}\Gamma\sum_{n\ell m}(-1)^\ell J_\ell(\lambda\,|z|)J_n(\tau)I_m(\tau) \times \{\cos[\lambda\,|z|\cos(\omega t-\pi/2)+\ell\omega t]K[(n+\ell-m)\hbar\omega] + \sin[\lambda\,|z|\cos(\omega t-\pi/2)+\ell\omega t]M[(n+\ell-m)\hbar\omega]\}, \tag{27}$$

$$K(\epsilon) = \tan^{-1}[\frac{eV+\epsilon+\tilde{E}_{\mathrm{d}}}{\Gamma/2}] - \tan^{-1}[\frac{\epsilon+\tilde{E}_{\mathrm{d}}}{\Gamma/2}],$$

$$M(\epsilon) = \frac{1}{2}\ln\{\frac{(eV+\epsilon+\tilde{E}_{\mathrm{d}})^2+\Gamma^2/4}{(\epsilon+\tilde{E}_{\mathrm{d}})^2+\Gamma^2/4}\}.$$

Equation (27) is exact and there is not necessarily restricted by $\lambda \ll 1$. For the symmetric situation, the terms associated with the approximation chosen as equation (25) are cancelled exactly. This equation is valid in the wide-band limit.

The time-averaged current I_α is obtained by integrating the time-dependent current over a period T, *i.e.*, $I_\alpha = \frac{1}{T}\int_0^T I_\alpha(t)\mathrm{d}t$. For arbitrary temperature, from

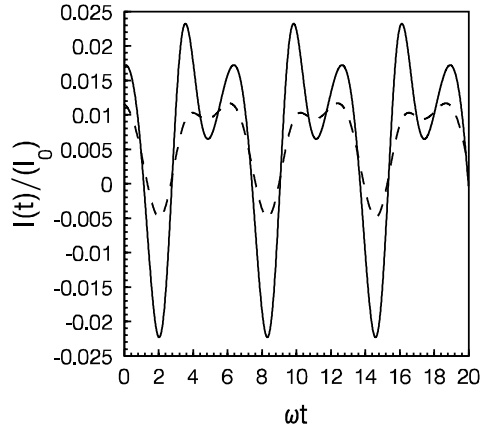

Fig. 1. Current oscillation *vs.* ωt tunneling through the quantum dot. The parameters are chosen as $\Gamma = 0.4\hbar\omega$, $\tilde{E}_{\rm d} = 1.5\hbar\omega$, $|Z| = 1$, $\phi = \pi/2$, $eV = 0.8\hbar\omega$, and (a) $\lambda = 0.302$ for the dashed curve; (b) $\lambda = 0.604$ for the solid curve.

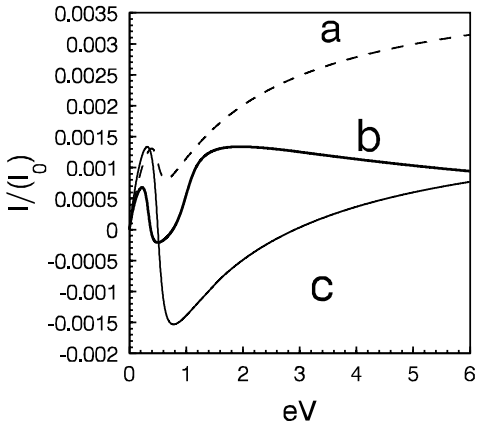

Fig. 2. Time-averaged net current *vs.* eV transporting through the quantum dot. The parameters are chosen as $\Gamma = 0.2\hbar\omega, |Z| = 1, \phi = \pi/2$, and (a) $\tilde{E}_{\rm d} = 1.5\hbar\omega$, $\lambda = 0.604$ for the dashed curve a; (b) $\tilde{E}_{\rm d} = 1.5\hbar\omega + 0.5eV$, $\lambda = 0.604$ for the solid curve b; (c) $\tilde{E}_{\rm d} = 1.5\hbar\omega$, $\lambda = 0.802$ for the solid curve c. eV is scaled by $\hbar\omega$.

equation (26) we obtain the time-averaged current in the αth lead for $\lambda \ll 1$ as

$$I_\alpha = -\frac{2e}{h}{\rm e}^{-\tau}\Gamma_\alpha {\rm Im}\sum_\sigma \int {\rm d}\epsilon \sum_{\ell nm} J_\ell(\lambda\,|\,z\,|)J_n(\tau)I_m(\tau) \times \{\tilde{R}_{\ell nm}(\epsilon) + J_\ell(\lambda\,|\,z\,|)f_\alpha(\epsilon)\tilde{G}^r_{d\sigma}[\epsilon - (n+\ell-m)\hbar\omega]\}, \tag{28}$$

where

$$\tilde{R}_{\ell nm}(\epsilon) = \frac{i}{2}{\rm e}^{-\tau}\sum_{qn_1m_1\ell_1}(-1)^\ell \Lambda[\epsilon - (n_1+\ell_1+m_1+n+\ell-m)\hbar\omega] \times J_{n_1}(\tau)I_{m_1}(\tau)J_{\ell_1}(\lambda\,|\,z\,|)J_q(\lambda\,|\,z\,|)J_{q+\ell+\ell_1}(\lambda\,|\,z\,|) \times \tilde{G}^r_{d\sigma}[\epsilon - (n-m-q)\hbar\omega]\tilde{G}^a_{d\sigma}[\epsilon - (n+\ell-m)\hbar\omega].$$

For the symmetric case, we obtain the time-averaged net current transporting through the quantum dot at zero temperature from equation (27) exactly

$$I = \frac{e}{h}{\rm e}^{-\tau}\Gamma\sum_{n\ell m} J^2_\ell(\lambda\,|\,z\,|)J_n(\tau)I_m(\tau)K[(n+\ell-m)\hbar\omega]. \tag{29}$$

Equations (27, 29) are the main results of this section which contain all the information of transport. They are exact in the symmetric tunneling system. The magnitude of the tunneling current is modulated by the exponential factor $\exp(-\tau)$.

We perform numerical calculation on the transport to show time-oscillating current and photon-assisted tunneling. As photon energy is much larger than thermal noise energy, quantum effect is obvious. In the following calculations we consider zero temperature transport and spin degenerate situation. We take wideband limit in the calculation, and deal with the symmetric case where $\Gamma_{\rm L} = \Gamma_{\rm R} = \Gamma/2$. The two quantities, $I_0 = \frac{2e\Gamma}{h}, G_0 = \frac{2e^2}{h}$, are defined as the measurement scale. All the energy quantities are scaled by the photon energy $\hbar\omega$.

We present the ac net tunneling current transporting through the quantum dot in Figure 1. The current evolves periodically with scaled time ωt. The configuration and magnitude of current is determined by the resonant feature of intrinsic structure of quantum dot, and by the external QMF. The oscillations are different due to different magnitudes of QMF. The solid curve is related to larger coupling strength $\Delta_{\rm d}$ than that of the dashed one. There are two kinds of tunneling oscillations for each of the net current. The main oscillation is split into two oscillations with the same period as that of the main oscillation. The period of the oscillation is not the same one as the period of QMF, but is a compound effect of electron resonance and applied QMF. The magnitude of the ac current increases with the strength of external QMF. We also see that the shapes of the vibrations are different due to different λ.

Figures 2 and 3 show the I-V characteristics of net dc tunneling current in different regions of bias voltage V. In these figures, we consider the situations for the gate voltage $V_{\rm g} = -\tilde{E}_{\rm d}/e$ is independent on the source-drain bias V, and is dependent on the bias V as $\tilde{E}_{\rm d} = \tilde{E}^{(0)}_{\rm d} + \frac{1}{2}eV$. Figures 2a and c are associated with the cases where the gate voltage is independent on source-drain bias, but with different coupling strength of QMF. As the bias $0 < eV < 0.6\hbar\omega$, there exists a peak in each of the curve. As $eV > 0.6\hbar\omega$ for curve a, and $eV > 0.75\hbar\omega$ for curve c, the tunneling dc current increases monotonically. The tunneling current is affected seriously by the external QMF. As the coupling strength of the field $\Delta_{\rm d}$ increases, the dc tunneling current may appear negative value. This phenomenon can not be observed in macroscopic systems, and it has not been reported for the system perturbed by CMF. Figure 2b is corresponding to the case where the gate voltage is dependent on the source-drain bias V.

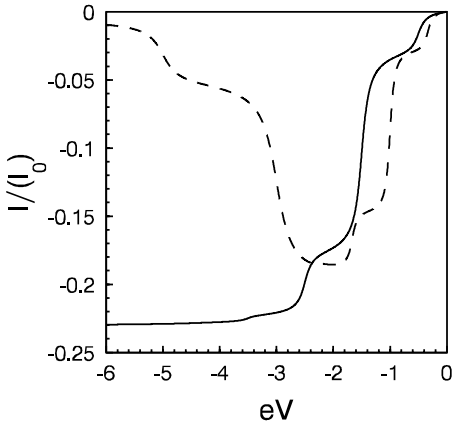

Fig. 3. Time-averaged net current *vs.* eV transporting through the quantum dot. This figure shows I-V characteristics in the negative voltage region. The parameters for solid curve are taken as the same ones in Figure 2a, while the parameters for dashed curve are the same as those in Figure 2b.

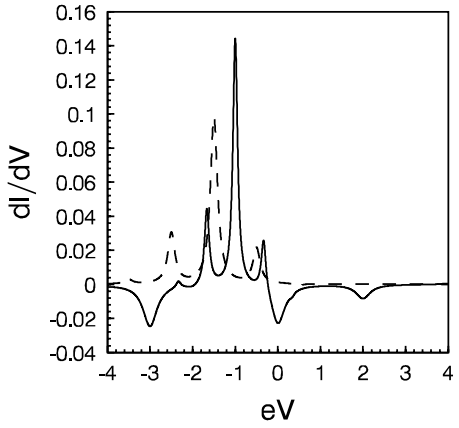

Fig. 4. The differential conductance $\mathrm{d}I/\mathrm{d}V$ *vs.* eV. The parameters are chosen as $\Gamma = 0.2\hbar\omega$, $|Z| = 1$, $\phi = \pi/2$, $\lambda = 0.604$ and (a) for the dashed curve $\tilde{E}_\mathrm{d} = 1.5\hbar\omega$; (b) for the solid curve $\tilde{E}_\mathrm{d} = 1.5\hbar\omega + 0.5eV$. The differential conductance is measured in the unit G_0, and eV is scaled by $\hbar\omega$.

There exist a current peak as $eV < 0.5\hbar\omega$ and small negative current value at the valley. The tunneling current increases in the region $0.5\hbar\omega < eV < 1.4\hbar\omega$, and then it decreases slowly and monotonically as $eV > 1.4\hbar\omega$. Figure 3 shows the dc tunneling current in the region $eV < 0$. The solid curve represents the case where gate voltage is not dependent on bias V, while the dashed curve represents the situation where gate voltage is related to source-drain bias by the relation $\tilde{E}_\mathrm{d} = 1.5\hbar\omega + \frac{1}{2}eV$. The tunneling current increases in the negative direction as the bias V increases negatively for the case where the gate voltage is not related to V, and it reaches to a saturate value. The tunneling current for the case where the gate voltage is related to V appears negative resonance in this region. In the diagrams, we see that there exist some current steps caused by the external QMF. They represent the process of photon-assisted tunneling. If the tunneling electrons absorb photons, they can jump to higher energy level. Thus some electrons gain enough energy to join the transport. This is a quantum effect, and it is well-known in CMF responsed systems. The steps become steep as Δ_d is large. The tunneling current is much larger in the negative region than the one in the positive region of V.

Figure 4 shows the structures of differential conductance *versus* the bias voltage V. The dashed curve corresponds to the tunneling current with gate voltage being independent on V, while the solid curve describes the current with gate voltage being related to the bias V. The diagrams exhibit resonant side peaks which are caused by the external QMF, they display photon-assisted tunneling. As the gate voltage is related to source-drain bias, the negative differential conductance *versus* V appears evidently. The behaviors of the tunneling current exhibit quite different feature on the mesoscopic transport for the two cases.

The time-averaged tunneling current versus gate voltage V_g is presented in Figure 5. There exist two shoulders beside the main peak if QMF is weak, and the shoulders become two side peaks as the coupling strength of QMF Δ_d increases. This is similar to the situation with CMF

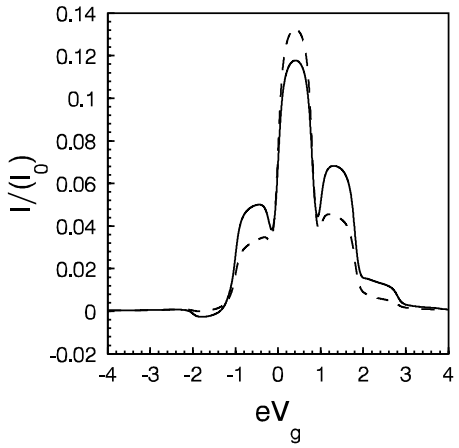

Fig. 5. The time-averaged net current transporting through the quantum dot *vs.* eV_g. The parameters are chosen as $\Gamma = 0.2\hbar\omega, |Z| = 1$, $\phi = \pi/2$, $eV = 0.8\hbar\omega$, and (a) for the dashed curve $\lambda = 0.604$; (b) for the solid curve, $\lambda = 0.802$. eV_g is scaled by $\hbar\omega$.

perturbed system. However, the resonant peaks exhibit fat appearances. The small negative tunneling current is also observed, and the negative current increases as the magnitude of QMF increases. Of course, the negative tunneling current disappears if QMF is removed.

The differential conductance corresponding to gate voltage V_g is shown in Figure 6. The negative conductance is seen obviously in several positions of eV_g. We observe that some peaks and valleys appear in addition to the main peak and valley. The heights and depths of the peaks and valleys are associated with the magnitude of QMF, and they become larger as QMF is stronger. The negative differential conductance is located in the regions where the valleys are found. The side peaks and side valleys will disappear as the external QMF is removed. For CMF applied system, the corresponding structures related

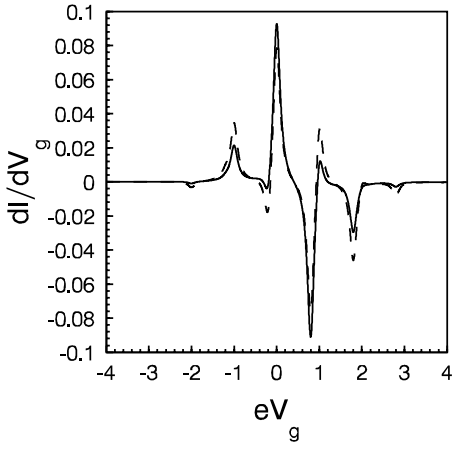

Fig. 6. The differential conductance $\mathrm{d}I/\mathrm{d}V_\mathrm{g}$ *vs.* eV_g. The parameters are chosen as $|z| = 1, \phi = \pi/2, eV = 0.8\hbar\omega, \Gamma = 0.2\hbar\omega$, and (a) for the solid curve $\lambda = 0.604$; (b) for the dashed curve $\lambda = 0.802$. The differential conductance is measured in the unit G_0, and eV_g is scaled by $\hbar\omega$.

to Figures 5 and 6 are reported in the literature, such as in reference [15] for considering two CMFs applying to the source and drain, and to the gate. However, our results reveal subtle quantum structures concerning CS.

4 The SU(1,1) coherent state expectation

We consider the EV over the SU(1,1) CS in this section. The realization of SU(1,1) Lie algebra for a single mode is $K_0 = (c^\dagger c + cc^\dagger)/4$, $K_+ = c^{\dagger 2}/2$ and $K_- = c^2/2$. For simplicity, we take EV over the squeezed number state $|\beta\rangle = S(\beta)\,|m\rangle$, where $|m\rangle$ is the usual number state, and $S(\beta)$ is the squeeze operator $S(\beta) = \exp(\frac{1}{2}\beta^* c^2 - \frac{1}{2}\beta c^{\dagger 2})$ with $\beta = |\beta|\exp(-i\phi)$. For the squeezed CS, the quantum fluctuation is smaller than the corresponding components of the CS. The photon number distributions for these states are oscillatory with zero probability for odd n (m = even) or for even n (m = odd) [31]. This state is a kind of nonclassical light field exhibiting nonclassical effect [30].

The following formulae are useful for our calculations

$$S^\dagger(\beta) c S(\beta) = \cosh(|\beta|)c - \exp(-i\phi)\sinh(|\beta|)c^\dagger, \quad (30)$$

$$S^\dagger(\beta)\hat{D}(\alpha)S(\beta) = \hat{D}(\gamma), \quad (31)$$

where

$$\gamma = \alpha\cosh(|\,\beta\,|) + \alpha^* \mathrm{e}^{-i\phi}\sinh(|\,\beta\,|).$$

The EV of the productor $\hat{P}^\dagger(t_1)\hat{P}(t_2)$ for our system can be derived as

$$\langle\beta|\,\hat{P}^\dagger(t_1)\hat{P}(t_2)\,|\beta\rangle = \zeta(t_2,t_1)\langle m|\,\hat{D}[\gamma(t_1,t_2)]\,|m\rangle. \quad (32)$$

The EV of the displacement over the usual number state $|m\rangle$ is given by

$$\langle m|\,\hat{D}(\gamma)\,|m\rangle = \exp(-\frac{1}{2}\,|\gamma|^2)L_m(|\gamma|^2), \quad (33)$$

where $L_m(x)$ are the Laguerre polynomials defined by

$$L_m(x) = \sum_{n=0}^{m}(-1)^n\frac{m!}{(n!)^2(m-n)!}x^n. \quad (34)$$

Substitute the value $\alpha(t_1,t_2) = \frac{i}{2}\lambda(\mathrm{e}^{i\omega t_2} - \mathrm{e}^{i\omega t_1})$ into $\gamma(t,t')$ in equation (31) we obtain

$$|\gamma(t_1,t_2)|^2 = \lambda^2\sin^2[\frac{1}{2}\omega(t_1-t_2)]\{\cosh(2|\beta|) + \sinh(2|\beta|)\cos[\omega(t_1+t_2)+\phi]\}. \quad (35)$$

Therefore, we can find the Keldysh Green function and tunneling current by taking EV over SU(1,1) CS. In our paper, we only consider the cases for SU(1,1) CS being two lowest states where $m = 0$, 1. It is not difficult to obtain the cases where $m > 1$.

4.1 EV over $|\,\beta\rangle = \mathbf{S}(\beta)\,|\mathbf{0}\rangle$

We consider EV of current operator over squeezed vacuum CS. As $m = 0$ the Laguerre polynomial $L_0(x) = 1$, and we have

$$\langle\beta|\,\hat{P}^\dagger(t_1)\hat{P}(t_2)\,|\beta\rangle = \zeta(t_2,t_1)\exp(-\frac{1}{2}\,|\gamma|^2). \quad (36)$$

The Keldysh Green function $\tilde{G}^<_{d\sigma}(t,t')$ is found as

$$\tilde{G}^<_{d\sigma}(t,t') = i\mathrm{e}^{-\tau_1}\int\frac{\mathrm{d}\epsilon}{2\pi\hbar}\Lambda(\epsilon)\sum_{n_1\ell_1\ell_2\ell_3\ell_4}(-1)^{\ell_3}\mathrm{e}^{i(\ell_2+\ell_3+\ell_4)\phi} \times J_{n_1}(\tau)I_{\ell_1}(\tau_1)I_{\ell_2}(\tau_2/2)I_{\ell_3}(\tau_2)I_{\ell_4}(\tau_2/2) \times G[\epsilon + (n_1-\ell_1-2\ell_2-\ell_3)\hbar\omega, t] \times G^*[\epsilon + (n_1-\ell_1+\ell_3+2\ell_4)\hbar\omega, t'], \quad (37)$$

where

$$G(\epsilon,t) = \mathrm{e}^{-\frac{i}{\hbar}\epsilon t}\tilde{G}^r_{d\sigma}(\epsilon), \qquad \tau = \frac{\lambda^2}{4},$$
$$\tau_1 = \tau\cosh(2\,|\,\beta\,|), \qquad \tau_2 = \tau\sinh(2\,|\,\beta\,|).$$

We take the approximation proposed in equation (25) to estimate the current in the leads as $\lambda \ll 1$. As mentioned in Section 3, this approximation does not affect the precision of net tunneling current for symmetric system. Finally, we arrive at the time-evolving current transporting from the αth lead into the quantum dot

$$I_\alpha(t) = -\frac{2e}{h}\Gamma_\alpha\mathrm{e}^{-\tau_1}\eta_1(t)\mathrm{Im}\sum_\sigma\int\mathrm{d}\epsilon\sum_{n\ell mp}(-1)^m J_n(\tau) \times I_\ell(\tau_1)I_m(\tau_2)I_p(\tau_2/2)\mathrm{e}^{i(m+p)(2\omega t+\phi)}\{W_{n\ell mp}(\epsilon,t) + f_\alpha(\epsilon)\tilde{G}^r_{d\sigma}[\epsilon - (n-\ell+m+2p)\hbar\omega]\}, \quad (38)$$

where

$$W_{n\ell mp}(\epsilon,t)=\frac{i}{2}\mathrm{e}^{-\tau_1}\sum_{n_1,\ell_1,..,\ell_4}(-1)^{\ell_3}J_{n_1}(\tau)I_{\ell_1}(\tau_1)I_{\ell_2}(\tau_2/2)\times I_{\ell_3}(\tau_2)I_{\ell_4}(\tau_2/2)\mathrm{e}^{i(\ell_2+\ell_3+\ell_4)(2\omega t+\phi)}\times\Lambda[\epsilon-(n_1-\ell_1+\ell_3+2\ell_4+n-\ell+m+2p)\hbar\omega]\tilde{G}^r_{d\sigma}\{\epsilon-[2(\ell_2+\ell_3+\ell_4+p)+n-\ell+m]\hbar\omega\}\tilde{G}^a_{d\sigma}[\epsilon-(n-\ell+m+2p)\hbar\omega],$$

and

$$\eta_1(t)=\exp[\frac{\tau_2}{2}\cos(2\omega t+\phi)].$$

For the symmetric system where $\Gamma_{\rm L}=\Gamma_{\rm R}$, the net ac tunneling current transporting through the quantum dot at zero temperature is given by the following analytical form

$$I(t)=\frac{e}{h}\Gamma\mathrm{e}^{-\tau_1}\eta_1(t)\sum_{n\ell mp}(-1)^m J_n(\tau)I_\ell(\tau_1)I_m(\tau_2)I_p(\tau_2/2)\times\{\sin[(m+p)(2\omega t+\phi)]M[(n-\ell+m+2p)\hbar\omega]+\cos[(m+p)(2\omega t+\phi)]K[(n-\ell+m+2p)\hbar\omega]\},\quad(39)$$

where $K(\epsilon)$ and $M(\epsilon)$ are defined by equation (27).

The time-averaged net tunneling current for the symmetric case is given by

$$I=\frac{e}{h}\Gamma\mathrm{e}^{-\tau_1}\sum_{n\ell mp}(-1)^m J_n(\tau)I_\ell(\tau_1)I_m(\tau_2)I_p(\tau_2/2)\times I_{m+p}(\tau_2/2)K[(n-\ell+m+2p)\hbar\omega].\quad(40)$$

Equations (39, 40) are two main results of this subsection. They are exact in the wideband limit, and they do not have the restriction as $\lambda\ll 1$. The ac tunneling current is modulated periodically with the envelope function $\eta_1(t)$. The magnitude of the current is also modulated by the factor $\exp(-\tau_1)$.

We present ac net tunneling current transporting through the quantum dot in Figure 7. The periodic oscillation of ac current is quite different from the oscillation shown in Figure 1. There are more oscillation peaks in this figure than in Figure 1. This means that the period in this figure is smaller than that of Figure 1. Between two larger peaks there exists one small peak. The magnitudes of the peaks are strongly dependent on the magnitude of QMF. The heights of these peaks increase as λ increases. Negative tunneling current may appear if the external QMF is strong enough. The solid curve represents the positive ac tunneling, while the dashed curve shows that negative tunneling appears periodically. Between two large peaks there exists one small peak.

We plot dc tunneling current *versus* gate voltage $V_{\rm g}$ in Figure 8. The resonant dc tunneling current structure is different from the one shown in Figure 5. In the presence of QMF, the slopes are modified to form steps. The steps become steeper and the main peak becomes lower as the applied QMF becomes stronger. There is no negative current in the net dc tunneling.

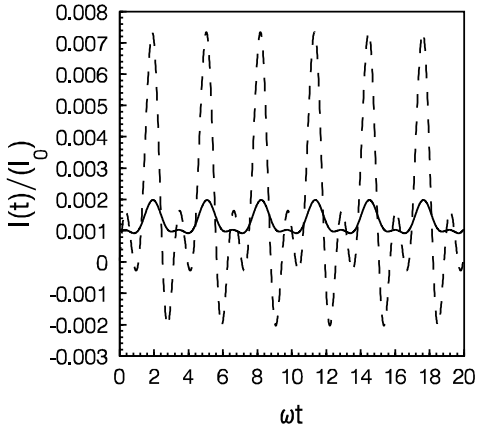

Fig. 7. The net tunneling current oscillation *vs.* ωt. The parameters are chosen as $\Gamma=0.4\hbar\omega$, $|\beta|=1$, $\phi=\pi/3$, $eV=0.8\hbar\omega$, $\tilde{E}_{\rm d}=2.5\hbar\omega$, and (a) $\lambda=0.302$ for the solid curve; (b) $\lambda=0.604$ for the dashed curve.

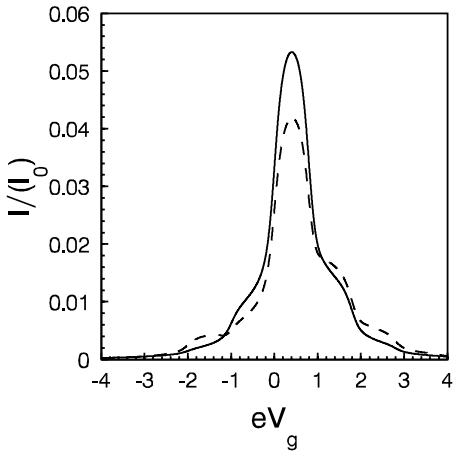

Fig. 8. The time-averaged net tunneling current *vs.* $eV_{\rm g}$. The parameters are chosen as $\Gamma=0.4\hbar\omega$, $|\beta|=1$, $eV=0.8\hbar\omega$, and (a) $\lambda=0.604$ for the solid curve; (b) $\lambda=0.802$ for the dashed curve. $eV_{\rm g}$ is scaled by $\hbar\omega$.

Figure 9 shows the differential conductance of tunneling current *versus* gate voltage $V_{\rm g}$. The negative conductance appears obviously due to the tunneling electrons resonating with quantum dot and with external QMF. The small peaks and valleys signify photon-assisted tunneling, while the main peak and valley are caused by the resonance of tunneling electron and local electron in the quantum dot. The small peaks and valleys become larger as QMF increases further, but the height and depth of the main peak and valley decrease. Comparing this figure with Figure 6, we see that they have similar structure. But in this figure, the base lines on which small resonant peaks located become bent.

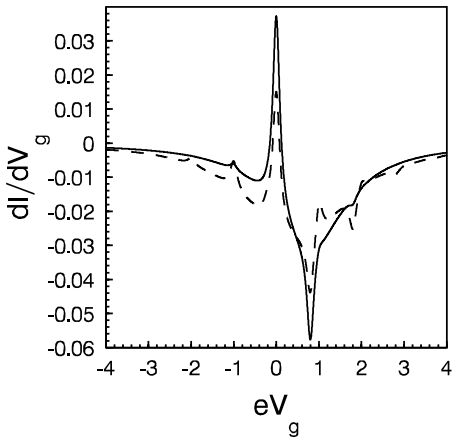

Fig. 9. The differential conductance $\mathrm{d}I/\mathrm{d}V_\mathrm{g}$ *vs.* eV_g. The parameters are chosen as $|\beta| = 1,\ \Gamma = 0.2\hbar\omega,\ eV = 0.8\hbar\omega$, and (a) $\lambda = 0.302$ for the solid curve; (b) $\lambda = 0.802$ for the dashed curve. The differential conductance is measured in unit G_0, and eV_g is scaled by $\hbar\omega$.

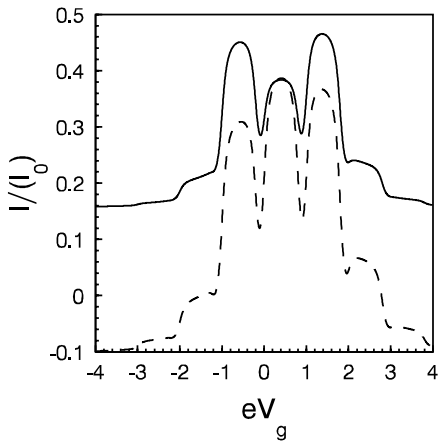

Fig. 10. The time-averaged net tunneling current *vs.* eV_g. The parameters are chosen as $\Gamma = 0.2\hbar\omega,\ |\beta| = 1,\ eV = 0.8\hbar\omega$, and (a) $\lambda = 0.604$ for the solid curve; (b) $\lambda = 0.802$ for the dashed curve. eV_g is scaled by $\hbar\omega$.

4.2 EV over $|\beta\rangle = S(\beta)\,|1\rangle$

We consider the lowest non-vacuum squeezed CS for the QMF applied system in this subsection. As m=1, we have the Laguerre polynomial $L_1(|\gamma|^2) = 1 - |\gamma|^2$. We consider the symmetric case where $\Gamma_\mathrm{L} = \Gamma_\mathrm{R}$. For this case, the time-averaged net tunneling current at zero temperature is expressed as the exact form

$$\begin{aligned} I = \frac{e}{\hbar}\Gamma \mathrm{e}^{-\tau_1} \sum_{n\ell mp} (-1)^m J_n(\tau) I_\ell(\tau_1) I_m(\tau_2) I_p(\tau_2/2) \\ \times \{\chi^{(1)}_{mp} K[(n-\ell+m+2p+1)\hbar\omega] \\ + \chi^{(2)}_{mp} K[(n-\ell+m+2p-1)\hbar\omega] \\ + \chi_{mp} K[(n-\ell+m+2p)\hbar\omega]\}, \end{aligned} \tag{41}$$

where

$$\begin{aligned} \chi_{mp} &= (1-2\tau_1) I_{m+p}(\tau_2/2) + \frac{\tau_2}{2}[I_{m+p+1}(\tau_2/2) \\ &\quad + I_{m+p-1}(\tau_2/2)], \\ \chi^{(1)}_{mp} &= \tau_1 I_{m+p}(\tau_2/2) - \tau_2 I_{m+p+1}(\tau_2/2), \\ \chi^{(2)}_{mp} &= \tau_1 I_{m+p}(\tau_2/2) - \tau_2 I_{m+p-1}(\tau_2/2). \end{aligned}$$

The current contains three major terms, each of which involves a main resonant peak but with different height. The magnitude of it is modulated by the factor $\exp(-\tau_1)$.

The time-averaged net tunneling current *versus* gate voltage is drawn in Figure 10. The solid curve and dashed curve correspond to the situations where $\lambda = 0.604$ and $\lambda = 0.802$, respectively. Comparing the diagrams with the case shown in Figue 8, we observe that the single resonant peak of current in the $S(\beta)\ |\,0\rangle$ state is split into three resonant peaks in the $S(\beta)\ |\,1\rangle$ state. The magnitudes of the three resonant peaks are strongly dependent on QMF. As the external QMF is strong enough, negative current may emerge. The absolute heights of peaks increase with the magnitude of QMF increases. The central peak grows more rapidly than the side peaks. The base of the tunneling current shifts down, and the shoulders rise as the magnitude of QMF increases. The current is negative when the bias $eV_\mathrm{g} < -2.5\hbar\omega$, or $eV_\mathrm{g} > 2.8\hbar\omega$ shown in the dashed curve. Compared with the situation in Figure 8, one can explain the fact as that the quantum state present more channels for electrons to transport. This is equivalent to the circumstance that many electrons transport through the quantum dot simultaneously and coherently. Each electron resonates in a channel.

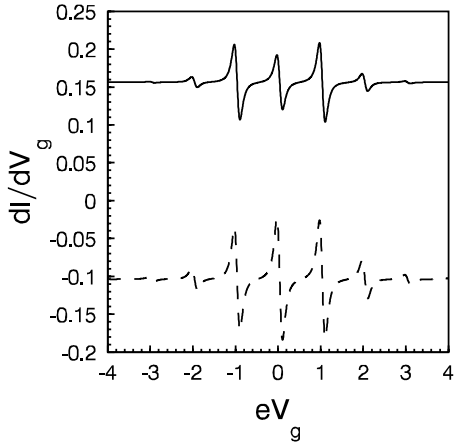

Fig. 11. The differential conductance $\mathrm{d}I/\mathrm{d}V_\mathrm{g}$ *vs.* eV_g. The parameters are chosen as $|\beta| = 1,\ \Gamma = 0.2\hbar\omega,\ eV = 0.8\hbar\omega$, and (a) $\lambda = 0.802$ for the dashed curve; (b) $\lambda = 0.604$ for the solid curve. The differential conductance is measured in unit G_0, and eV_g is scaled by $\hbar\omega$.

Figure 11 represents the resonant behaviors of differential conductance *versus* gate voltage. Comparing with the diagrams in Figure 9, we see that three main peaks and valleys emerge in the central region. Each of the main

peaks is associated with one of the main peaks presented in Figure 10. The diagram of the differential conductance shifts down, and the magnitudes of peaks and valleys increase as the strength of QMF increases. The negative differential conductance do not occur as QMF is weak, but it takes place as QMF is strong enough. The small peaks and valleys correspond to the shoulders in Figure 10.

5 Concluding remarks

We have examined the tunneling current through a quantum dot perturbed by a QMF. The time-dependent and time-averaged tunneling current formulae are obtained analytically. The differential conductances $\mathrm{d}I/\mathrm{d}V$ and $\mathrm{d}I/\mathrm{d}V_\mathrm{g}$ are studied at zero temperature. The special cases are discussed by considering wideband limit and symmetric interaction between the quantum dot and the two leads. The main analytical current formulae are equations (27, 29) related to CS, and equations (39, 40, 41) related to SU(1,1) CS. The photon-assisted tunneling and resonant behaviors are observed in the QMF applied system. Negative differential conductance is also exhibited. Some of the similar phenomena are already known in CMF applied systems. However, in the QMF applied system, the tunneling current formulae and the differential conductance formulae are much complicated because of the quantum fluctuation. So that new effects are hidden in the formulae. The quantum signal applying to the quantum devices may transfer information to the tunneling current, and all the measurable quantities fluctuate around their mean values. This induces quantum noise in the system. The coherent phases are modified by the quantum field. Therefore, the transport behaviors appear compound effect due to the resonant tunneling and quantum environment. We have investigated the CS and SU(1,1) CS QMFs perturbed systems. These two field states are well-known in quantum optics, while they have not been employed in quantum dot system before. The current is related to the applied QMF sensitively. It appears different behaviors for different QMF. For the system concerned with CS and squeezed vacuum state, the dc tunneling behaviors are somewhat similar to the system applied by CMF. However, for the system related to other squeezed CS, the tunneling current appears quite new effect. The main resonant peak splits to form multi-resonant state. This provides more resonant channels for electrons to tunnel. The magnitude of the current is modulated by QMF in the exponential form, and the modulation is intimately related to the quantum state. In this paper, we only consider symmetric tunneling, and have obtained photon-assisted transport. As the source-drain bias is zero, there is no tunneling current. For this symmetric interaction system, there is no photon-electron pump effect. This is because the pumped electrons can tunnel to both leads equivalently. As the restriction $\Gamma_\mathrm{L} = \Gamma_\mathrm{R}$ is removed, we can find the photon-electron pump effect. Dynamic behaviors of the tunneling current exhibits quite different time-evolution structure for different QMF state. As the coupling strength Δ_d is zero, the current formulae reduce to Landauer-Büttiker formula with resonant Breit-Wigner single energy form.

Quantum dot is an ideal model of the quantum device with very small sizes in three dimensions. Electrons tunneling through the device are coherent and correlated with the external perturbation. The quantum device responds sensitively to the quantum nature of different external QMF. There is no classical correspondence for the fully quantum theory, because our system is quite different from the classical version where CMFs are imposed on quantum devices. As the devices are applied with light signals, the fluctuations of magnitudes and phases of the light signals can result in uncertainty during the measurements. The fluctuations are mainly caused by quantum fluctuation of field nature.

One of the authors (H.K. Zhao) wishes to thank M. Wagner, B. Kramer, C. Bruder, and M. Stopa for communications. This work was supported by RGC of SAR Government of Hong Kong under Grant No. HKU 7112/97P, and by the National Natural Science Foundation of China under Grant No. 19875004.

References

1. *Quantum coherence in mesoscopic systems*, Vol. 254 of NATO Advanced Study Institute, Series B: Physics, edited by B. Kramer (Plenum, New York, 1991).
2. *Mesoscopic phenomena in solids*, edited by B.L. Altshuler, P.A. Lee, R.A. Webb (Amsterdam: Elsevier, 1991); Y. Imry, *Introduction to mesoscopic physics* (Oxford: Oxford University Press, 1997).
3. R. Landauer, IBM J. Res. Dev. **1**, 223 (1957); M. Büttiker, Phys. Rev. Lett. **57**, 1761 (1986).
4. M. Büttiker, A. Pretre, H. Thomas, Phys. Rev. Lett. **70**, 4114 (1993); T. Christen, M. Büttiker, Phys. Rev. Lett. **77**, 143 (1996); T. Gramespacher, M. Büttiker, Phys. Rev. B **56**, 13026 (1997).
5. Y. Meir, N.S. Wingreen, P.A. Lee, Phys. Rev. Lett. **70**, 2601 (1993); C.W.J. Beenakker, B. Rejaei, J.A. Melsen, Phys. Rev. Lett. **72**, 2470 (1994); A. Schiller, S. Hershfield, Phys. Rev. B **51**, 12896 (1995).
6. F. Zhou, B. Spivak, N. Taniguchi, B.L. Altshuler, Phys. Rev. Lett. **77**, 1958 (1996); O. Agam, N.S. Wingreen, B.L. Altshuler, D.C. Ralph, M. Tinkham, Phys. Rev. Lett. **79**, 1956 (1997).
7. J. Yi, M.Y. Choi, K. Park, E.H. Lee, Phys. Rev. Lett. **78**, 3528 (1997); Y. Naveh, D.V. Averin, K.K. Likharev, Phys. Rev. Lett. **79**, 3482 (1997); R. Fazio, R. Raimondi, Phys. Rev. Lett. **80**, 2913 (1998).
8. H.K. Zhao, J. Phys. A **29**, 5827 (1996); H.K. Zhao, Commun. Theor. Phys. **29**, 33 (1998); J. Wang, Q.R. Zheng, H. Guo, Phys. Rev. B **55**, 9770 (1997); Z.S. Ma, J. Wang, H. Guo, Phys. Rev. B **57**, 9108 (1998).
9. F.W.J. Hekking, L.I. Glazman, K.A. Matveev, R.I Shekhter, Phys. Rev. Lett. **70**, 4138, (1993).
10. J.A. Folk *et al.*, Phys. Rev. Lett. **76**, 1699 (1996); S.M. Cronenwett *et al.*, Phys. Rev. Lett. **79**, 2312 (1997).
11. C. Bruder, H. Schoeller, Phys. Rev. Lett. **72**, 1076 (1994); Ph. Brune, C. Bruder, H. Schoeller, Phys. Rev. B **56**, 4730 (1997).

12. P.F. Bagwell, R.K. Lake, Phys. Rev. B **46**, 15329 (1992); A. Schiller, S. Hershfield, Phys. Rev. Lett. **77**, 1821 (1996).
13. L.P. Kouwenhoven *et al.*, Phys. Rev. Lett. **73**, 3443 (1994); T.H. Oosterkamp *et al.*, Phys. Rev. Lett. **78**, 1536 (1997).
14. M. Wagner, Phys. Rev. A, **51**, 798 (1995); M. Wagner, Phys. Rev. Lett. **76**, 4010 (1996).
15. T.H. Stoof, Yu.V. Nazarov, Phys. Rev. B **53**, 1050 (1996); Q.F. Sun, T.H. Lin, Phys. Rev. B **56**, 3591 (1997).
16. H.K. Zhao, Z. Phys. B **102**, 415 (1997); H.K. Zhao, Phys. Lett. A **226**, 105 (1997); H.K. Zhao, G.v. Gehlen, Phys. Rev. B **58**, 13660 (1998).
17. B.J. Keay *et al.*, Phys. Rev. Lett. **75**, 4102 (1995); G. Platero, R. Aguado, Appl. Phys. Lett. **70**, 3546 (1997).
18. J. Iñarren, G. Platero, C. Tejedor, Phys. Rev. B **50**, 4581 (1994); R. Aguado, J. Iñarrea, G. Platero, Phys. Rev. B **53**, 10030 (1996).
19. L.J. Geerlings *et al.*, Phys. Rev. Lett. **64**, 2691 (1990).
20. C.A. Stafford, N.S. Wingreen, Phys. Rev. Lett. **76**, 1916 (1996).
21. P.K. Tien, J.P. Gordon, Phys. Rev. **129**, 647 (1963).
22. A-P. Jauho, N.S. Wingreen, Y. Meir, Phys. Rev. B **50**, 5528 (1994).
23. A. Vourdas, Phys. Rev. B **49**, 12040 (1994); A. Vourdas, Z. Phys. B **100**, 455 (1996); L.M. Kuang, Y. Wang, M.L. Ge, Phys. Rev. B **53**, 11764 (1996).
24. N.S. Wingreen, A-P. Jauho, Y. Meir, Phys. Rev. B **48**, 8487 (1993).
25. Z.S. Ma, J. Wang, H. Guo, Phys. Rev. B **59**, 7575 (1999).
26. Currently, the general gauge invariant theory for finite frequency and finite voltage bias is not available. For the recent development of the gauge invariant theory, see M.H. Pedersen, M. Büttiker, Phys. Rev. B **58**, 12993 (1998).
27. L.B. Keldysh, Zh. Eksp. Teor. Fiz. **47**, 1515 (1964) [Sov. Phys. JETP **20**, 1018 (1965)].
28. L.Y. Chen, C.S. Ting, Phys. Rev. B **44**, 5916 (1991).
29. T.K. Ng, Phys. Rev. Lett. **77**, 487 (1996).
30. R. London, P.L. Knight, J. Mod. Opt. **34**, 709 (1987); D.F. Walls, Nature **306**, 141 (1983).
31. C.C. Gerry, J. Opt. Soc. Am. B **8**, 685 (1991); M.S. Kim, F.A.M. de Oliveira, P.L. Knight, Phys. Rev. A **40**, 2494 (1989).